Research article

JHEP|Reports

Single-cell transcriptomics reveals the impact of sex and age in the healthy human liver

Authors

Raza Ur Rahman, Eliana T. Epstein, Shane Murphy, …, Angela Shih, Jacques Deguine, Alan C. Mullen

Correspondence

alan.mullen@umassmed.edu (A.C. Mullen).

Graphical abstract

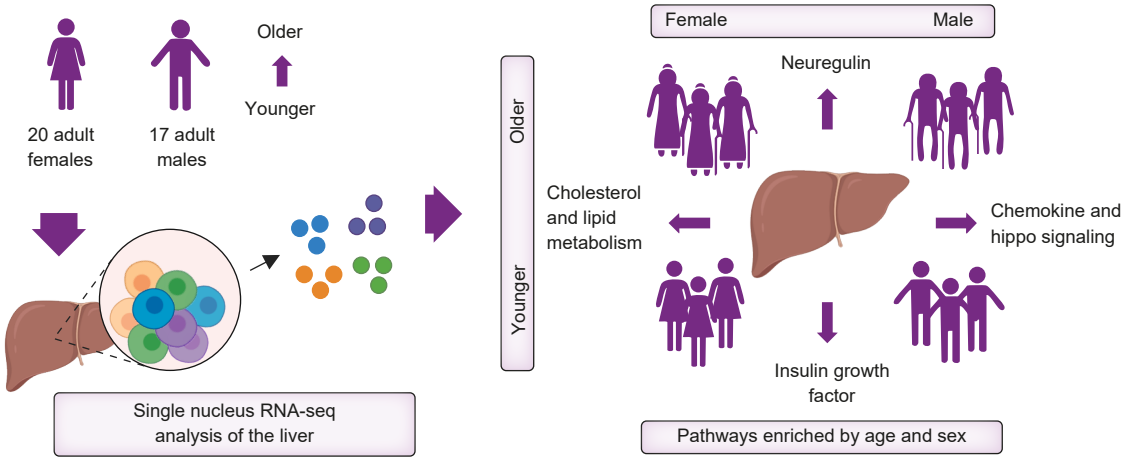

Highlights:

- Single-nucleus RNA-seq of 37 healthy human livers reveals sex- and age-related gene expression differences.
- Sex influences signaling pathways: lipid metabolism enriched in females and BMP signaling enriched in males.
- Age-related liver changes: IGF pathways enriched in younger and neuregulin signaling in older individuals.

Impact and implications:

Our study provides a comprehensive single-cell analysis of 37 healthy human liver samples, revealing how sex and age influence gene expression profiles, cellular interactions, and signaling responses across liver cell types and subtypes. These insights are of particular significance for researchers investigating the influence of sex and age on cellular responses to injury and treatment of injury. Furthermore, this dataset serves as a healthy reference, enabling future studies to understand how ancestry, geography, and disease states shape liver biology in the context of age and sex.

https://doi.org/10.1016/j.jhepr.2026.101773

JHEP|Reports

Single-cell transcriptomics reveals the impact of sex and age in the healthy human liver

Raza Ur Rahman[1,2], Eliana T. Epstein[3], Shane Murphy[2,4], Liat Amir-Zilberstein[2,4], Cristin McCabe[2,4], Toni M. Delorey[2,4], Hope Koene[3], Lilly Fernandes[3], Kenneth K. Tanabe[5], Motaz Qadan[5], Cristina R. Ferrone[5,†], David L. Berger[5], Angela Shih[6], Jacques Deguine[2,4], Alan C. Mullen[1,2,*]

JHEP Reports **2026**. vol. 8 | 1–13

Background & Aims: The liver is a vital organ composed of parenchymal, non-parenchymal, and immune cell populations. Single-cell sequencing approaches now provide the opportunity to understand how sex and age influence gene expression and cellular function across cell types within the liver.

Methods: We analyzed the cellular composition and intercellular interactions of the human liver through single-nucleus RNA sequencing, incorporating insights from 37 healthy liver samples. The dataset contains cells from female and male donors spanning more than seven decades of life, and analysis was performed to evaluate the impact of sex and age on differential gene expression, pathway enrichment, and predicted ligand-receptor and protein-protein interactions.

Results: Excluding the X and Y chromosomes, we identified 374 genes uniquely enriched in cells of the female liver and 520 genes enriched in cells of the male liver. Differential expression analysis defined unique circuitries enriched within each cell type between females and males and their impact on cell-cell communication and response to external signals, including enrichment of cholesterol metabolism (p <1.64 x 10^{-3}), TGF-β receptor signaling (p <5.69 x 10^{-3}), and fibronectin production (p <1.04 x 10^{-8}) in female cells and bone morphogenic protein signaling (p <7.62 × 10^{-6}) in male cells. With increasing age, we observe a greater diversity in gene expression, including enrichment of genes that regulate neuregulin signaling (p <7.81 × 10^{-3}) at older ages, while genes regulating insulin growth factor signaling (p <2.44 × 10^{-3}) are enriched at younger ages. Senescence signatures were also identified for each cell type within the liver.

Conclusions: These results define the activities of healthy cell types within the liver across sex and age, providing a foundation for studies to examine how ancestry, geography, and disease states influence liver function within these contexts.

Introduction

The liver performs diverse metabolic, synthetic, and immune functions through specialized cell types. Single-cell RNA sequencing (scRNA-seq) has illuminated this cellular diversity,[1–3] but understanding how sex and age shape hepatic function remains limited by small cohort sizes and underrepresentation of hepatocytes and other non-immune cell populations in human scRNA-seq datasets.

Here, we present a comprehensive map of the cellular composition of the human liver through single-nucleus RNA sequencing (snRNA-seq), which provides a broader representation of hepatocytes and other non-immune cell types compared to scRNA-seq. We analyzed data from 37 healthy liver samples (>195,000 nuclei) across seven decades of life from both female and male donors. This study demonstrates the influence of sex and age on gene expression, advances our understanding of cellular heterogeneity in the liver, and establishes a foundation for future research into the mechanisms underlying sex- and age-related disease progression.

Materials and methods

snRNA sequencing and analysis

Samples were prepared and processed for snRNA-seq as previously described[4] and detailed in the supplementary methods. snRNA-seq data were processed using Cell Ranger v7.0.1, with ambient RNA removal (SoupX version 1.6.2) and doublet filtering (DoubletFinder v2.0.4), followed by integration (Harmony v1.2.0), clustering and visualization (Seurat v4.3.0), and cell type annotation (ScType R package with 'ScTypeDB_full.xlsx' database). Differential expression analysis employed the MAST test in Seurat v4.3.0 (FindMarkers) comparing sex and age groups with donor and demographic variables as latent factors. Gene ontology enrichment used

* Corresponding author. Address: Lazare Research Building, University of Massachusetts Chan Medical School, Worcester, MA 01605, USA. Tel.: (508) 856-4005.
E-mail address: alan.mullen@umassmed.edu (A.C. Mullen).
† Current Address: Cristina R. Ferrone, Department of Surgery, Cedars-Sinai Medical Center, Los Angeles, California
https://doi.org/10.1016/j.jhepr.2026.101773

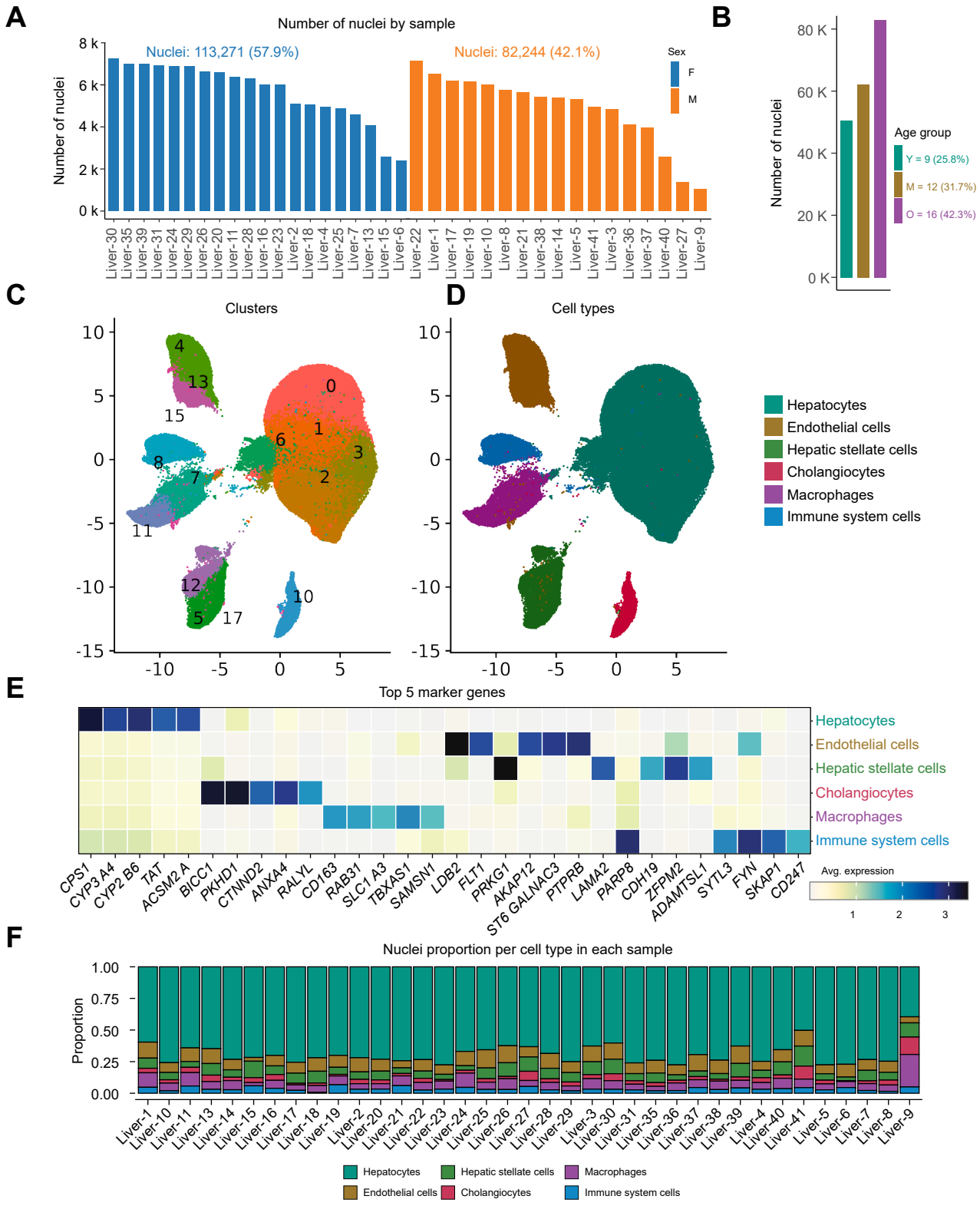

Fig. 1. Sample composition, clustering, and cell-type proportions in human liver samples. (A) Nuclei counts are shown for each sample and separated by sex (female in blue and male in orange). (B) Nuclei counts are shown for each age group. Younger (18-40 years, teal), middle (41–60 years, brown), and older (>60 years, purple). (C) UMAP of nuclei clustered at resolution 0.5. Each point represents an individual nucleus, colored according to its assigned cluster. Cluster identities are labeled numerically to correspond with specific populations identified in the analysis. (D) UMAP from C colored by cell type. (E) Top 5 marker genes defining each cell type identified in D. (F) Proportions of each cell type across all samples. UMAP, uniform manifold approximation and projection.

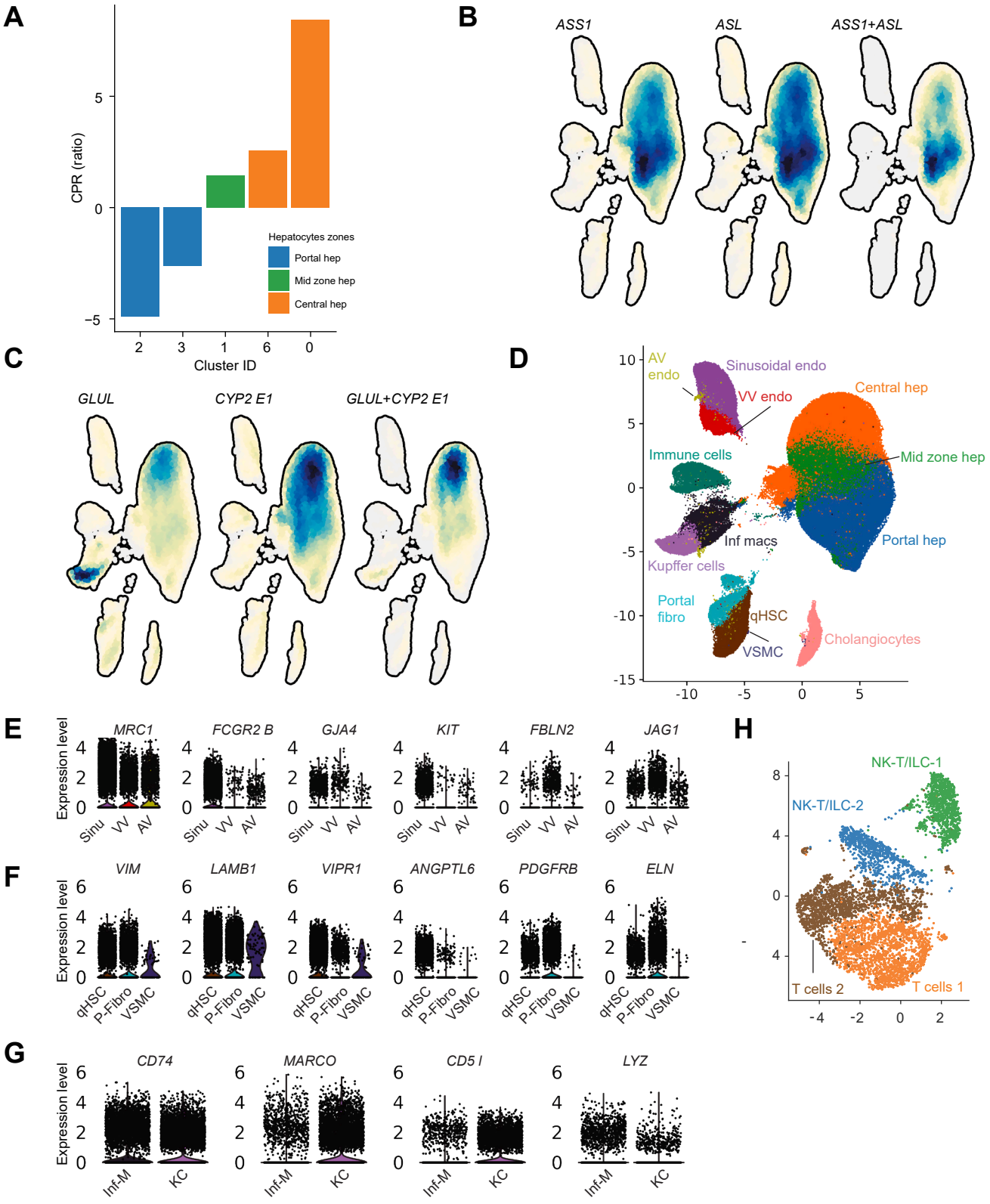

Fig. 2. Defining hepatocyte zonation and non-hepatocyte subtypes. (A) CPR for hepatocyte clusters, calculated using zonal markers *ASS1*, *ASL* (portal), and *GLUL*, *CYP2E1* (central). Clusters were classified as portal (CPR values ≤ lower quantile: clusters 2, 3), central (CPR values ≥ upper quantile: clusters 0, 6), or mid-zone (intermediate CPR values: cluster 1). (B) UMAP density plots of *ASS1* and *ASL* expression with a joint co-expression density plot. (C) UMAP density plots of *GLUL* and *CYP2E1* expression with a joint co-expression density plot. (D) UMAP visualization of cell types and subtypes within the liver. (E-G) Marker genes identifying subtypes of the indicated populations in D. (H) UMAP visualization of non-macrophage immune subtypes. CPR, central-to-portal ratio; UMAP, uniform manifold approximation and projection.

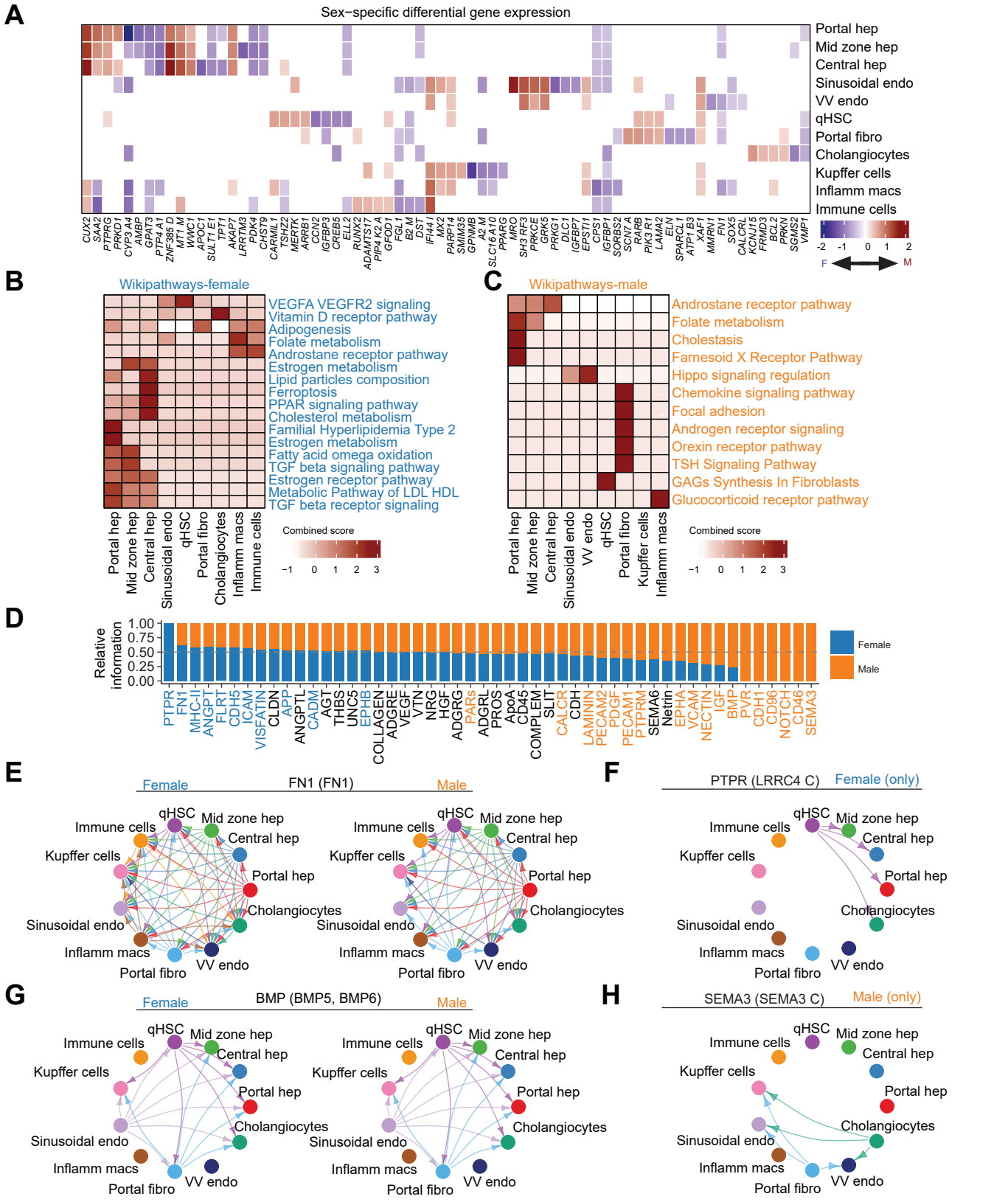

Fig. 3. Sex-specific gene expression, pathway enrichment, and signaling. (A). Heatmap displaying the log_2FC in gene expression between females and males across liver cell types and subtypes. Red indicates higher expression in males; blue signifies higher expression in females. For each cell type/subtype, the top four differentially expressed genes upregulated in females or males and expressed in ≥25% of cells are shown. Genes were called significant within a cell type if detected in ≥10% of cells in either sex (min.pct = 0.1), $|log_2FC| \geq 0.25$, and Bonferroni-adjusted *p*-value (*p*_val_adj) ≤0.1. (B) Biological processes (Wiki pathways) enriched in differentially expressed genes across cell types in females. The combined score was calculated by logarithmically transforming the *p* value from Fisher's exact test

EnrichR version 3.2 (WikiPathway_2023_Human library), cell-cell communication was analyzed with CellChat v2.1.2, protein-protein interactions were examined using STRINGdb v2.10.1 (STRING database species = 9,606, version = 11.5), and cell-type proportions were assessed with speckle R package v0.99.7. Detailed methodological parameters and workflows are provided in the supplementary methods.

Results

Charting the human liver landscape with snRNA-seq

We analyzed nuclei from 20 female (113,271) and 17 male (82,244) donors (Fig. 1A, Table S1) across seven decades of life (Fig. 1B and S1). Nuclei from all samples were integrated and clustered at multiple resolutions (Figs. S2 and S3A), and a resolution of 0.5 was selected for downstream analyses (Fig. S3A, supplementary methods). Clusters 9, 14, and 16 were removed during quality control (Table S2, Fig. S3B, supplementary methods). Clusters were annotated using ScType[5] with the liver as the target tissue (Fig. 1C, D, Table S3) and cross-referenced to annotation with CellTypist[6] (Fig. S4, Table S3, supplementary methods). Marker genes for each cell type and their distribution across individual samples are shown (Fig. 1E-F, Tables S3 and S4).

Evaluating hepatocyte zonation

We next classified hepatocytes into portal, central, and mid-zone based on the expression of the zonal markers: *ASS1*, *ASL*, *GLUL,* and *CYP2E1*.[7] We calculated the central-to-portal ratio for each hepatocyte sub-cluster (Fig. 1C) by subtracting the summed expression of *ASS1* and *ASL* (portal) from the summed expression of *GLUL* and *CYP2E1* (central) for each hepatocyte sub-cluster (Fig. 2A, Table S5, supplementary methods). This classification was validated with UMAP (uniform manifold approximation and projection) visualization and confirmed with density plots (Fig. 2B,C). Portal, mid-zone, and central hepatocytes were then annotated within the overall UMAP (Fig. 2D).

Defining non-hepatocyte cell types and subtypes

We evaluated each individual non-hepatocyte cluster (Fig. 1C) to define cell types and subtypes. We identified sinusoidal, venous vascular (VV), and arterial vascular endothelial cells[8] (Fig. 2E, Table S6). Hepatic stellate cells (HSCs) were separated into quiescent HSCs (qHSCs) and portal fibroblasts,[9] and a population of vascular smooth muscle cells was annotated (Fig. 2F). Macrophages were separated into Kupffer-like cells (*CD74*^{high}, *MARCO*^{high}, *CD5L*^{high}) and inflammatory macrophages (*CD74*^{high}, *LYZ*^{high}, *MARCO*^{low})[1] (Fig. 2G). Cell types were evenly distributed across samples (Fig. S5, supplementary methods), with balanced representation across sexes (Fig. S6) and age groups (Fig. S7).

The non-macrophage immune system cell population (6,544 nuclei) was then sub-clustered from the raw data using the same analysis pipeline and annotated with the ScType tool using Immune System Cells as the target tissue (Fig. 2H, Table S7) and Celltypist (Fig. S8, Table S7). Both approaches identified two T cell clusters but annotated the other clusters as NK-T cells and innate lymphoid cells, respectively (supplementary methods).

Effect of sex on differential gene expression and biological pathways

Cell type proportions were analyzed (Table S8, supplementary methods) and differential expression analysis across cell types was performed with donor and age as covariates. We identified 425 genes upregulated in females and 581 genes upregulated in males, with 37 genes upregulated in both sexes, but in distinct cell types (Table S9). When focusing on autosomal genes (excluding X and Y chromosomes), 374 genes were upregulated in females, 520 in males, and 36 genes were upregulated across both sexes, again in distinct cell types. We focused on autosomal genes for the subsequent analyses. The top four most enriched genes in female and male cell types were plotted (Fig. 3A).

We next examined biological processes enriched across cell types based on differential gene expression between female and male cells (Fig. 3B and Table S10). The estrogen receptor pathway, estrogen metabolism, and TGF-β signaling were enriched in female hepatocytes. Pathways related to lipid and cholesterol metabolism were also upregulated in female hepatocytes. Vitamin D receptor signaling was enriched in cholangiocytes, VEGFA–VEGFR2 signaling in qHSCs, and folate metabolism in inflammatory macrophages and other non-macrophage immune cell populations.

In male cells, the Farnesoid X Receptor Pathway was enriched in portal hepatocytes, while Chemokine Signaling, the Orexin Receptor Pathway, and Focal Adhesion were enriched in portal fibroblasts. The Glucocorticoid Receptor Pathway was enriched in inflammatory macrophages, whereas the Hippo Signaling Regulation Pathway was enriched in both sinusoidal and VV endothelial cells (Fig. 3C, Table S10).

Common pathways were enriched across multiple cell types in both females and males, including the androstane receptor pathway and folate metabolism (Fig. 3B,C, Table S10). These findings highlight both sex-specific pathway enrichment in healthy liver cell populations and the differential effects of shared pathways on cellular activity between females and males.

and multiplying it by the z-score. Terms were considered significantly enriched at a Benjamini-Hochberg false discovery rate (FDR) of ≤0.1 with ≥3 contributing genes. (C) Biological processes enriched in differentially expressed genes across cell types in males. Terms were considered significantly enriched at a Benjamini-Hochberg FDR of ≤0.1 with ≥3 contributing genes. (D) Signaling pathways were ranked according to differences in overall information flow between female and male communication networks. Statistical signficance was assessed using a paired Wilcoxon test, with $p \leq 0.05$ considered signficant. Blue pathways are more enriched in females, orange in males, and black show no sex-specific enrichment. (E–H) Chord circle plots show selected significantly interacting pathways from panel D and their communication probabilities: (E) FN1 signaling with FN1 as the enriched ligand. Colors indicate the cell-type expressing the ligand, and the strength of communication is indicated by the thickness of the line; (F) PTPR signaling (only in females) with LRRC4C as the enriched ligand; (G) BMP signaling with BMP5 and BMP6 as enriched ligands; and (H) SEMA3 signaling (only in males) with SEMA3C as the enriched ligand. FC, fold change; FDR, false discovery rate; GAGs, glycosaminoglycans; qHSCs, quiescent hepatic stellate cells; VV, venous vascular.

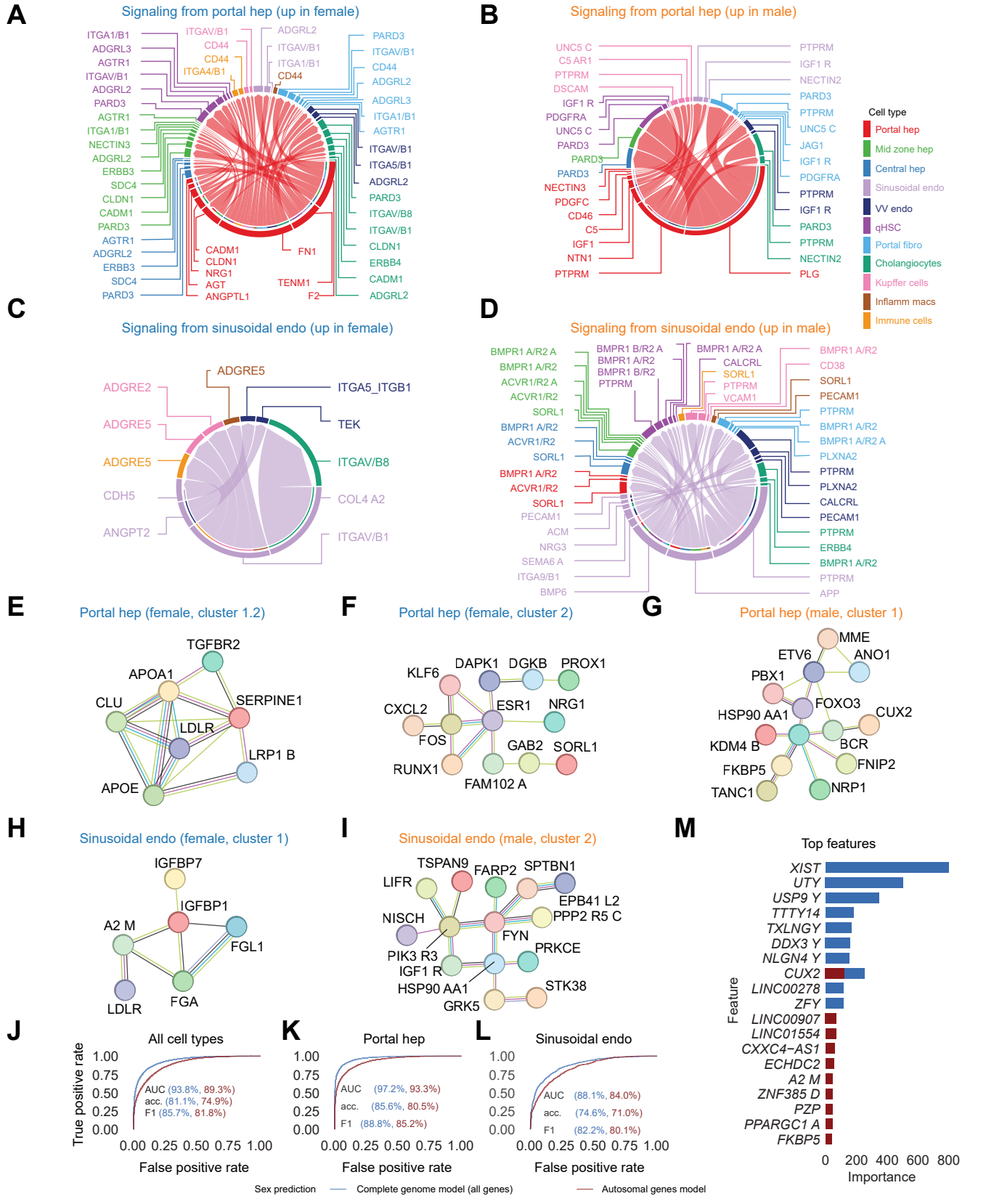

Fig. 4. Sex-specific intercellular interactions, protein networks, and application of machine learning. (A-D) Chord diagrams represent sex-specific L-R interactions. Outer rings denote different cell types; links connect source (ligand-expressing) to target (receptor-expressing) cell types. L–R signaling from portal hepatocytes enriched in females (A) and males (B), and from sinusoidal endothelial cells enriched in females (C) and males (D). (E-H) STRINGDB network analysis of protein-protein interactions. Nodes represent proteins, while edges (lines) depict interactions, colored by evidence source (Red: fusion evidence, Green:

Impact of sex on cell-cell communication

We used CellChat (v2) to estimate signaling pathway strength among cell groups (Fig. 3D, Table S11). Female cells showed enrichment in PTPR, ANGPT, FN1, and VISFATIN pathways (Fig. 3D, blue labels), while male cells were enriched in SEMA3, VECAM, IGF, BMP, and PDGF pathways (orange labels). Additional pathways are active but showed no significant sex-specific differences (Fig. 3D, black labels).

Cell-cell communication maps (Table S11) showed enriched FN1 signaling from female hepatocytes (Fig. 3E). However, most hepatocyte-derived FN1 is secreted into plasma,[10] so its impact on other resident liver cells is uncertain. After removing hepatic FN1 from the analysis (Fig. S9), FN1 expression remained female-enriched. Portal fibroblasts continued to signal to vascular (VV) and sinusoidal endothelial as well as immune populations. Additionally, we observed FN1 signaling originating from cholangiocytes, immune cells, and inflammatory macrophages. PTPR signaling was only enriched between female cells (Fig. 3F). In contrast, BMP signaling was enriched in males (Fig. 3G), and the SEMA3 pathway was active in males without active signals identified in females (Fig. 3H).

To identify molecules driving cell-cell interactions, we next visualized ligand-receptor (L-R) pairs enriched in female and male cell types (Fig. 4A-D, Table S11). The analysis focused on signaling from portal hepatocytes and sinusoidal endothelial cells as examples, and the full results are provided in Table S11. In female portal hepatocytes, L-R pairs containing the ligands ANGPTL1, TENM1, AGRL3, CADM1, and FN1 were enriched, while in male portal hepatocytes, L-R pairs containing the ligands IGF1, PLG, and NTN1 were enriched. In female sinusoidal cells, L-R pairs containing the ligands ANGPT2 and COL4A2 were enriched (Fig. 4C), while L-R pairs containing the ligands BMP6 and APP were enriched in males (Fig. 4D).

Influence of sex on protein networks

We next predicted differences in protein-protein interactions between female and male cell types. We focused on networks within hepatocytes and endothelial cells for visualization and included all data for interactions and subcellular compartments in Table S12. In female portal hepatocytes, the subnetwork containing APOA1, APOE, LDLR, and LRP1B (Fig. 4E) was enriched for pathways related to lipid particle composition, LDL, HDL, and triglyceride metabolism, as well as familial hyperlipidemia (Table S12). The associated proteins are primarily localized to lipoprotein particles or are lipoprotein receptors (LDLR and LRP1) (Table S12). A protein network in female portal hepatocytes was also identified that centered on ESR1 and FOS (Fig. 4F). This network was enriched in estrogen signaling, and ESR1-containing networks were also present in central and mid-zone hepatocytes (Fig. S10). Proteins in this network are primarily localized to the nucleus and include nuclear receptors and intermediate signaling molecules (Table S12).

An additional protein network enriched in female portal hepatocytes included ADH1A, ADH1B, CYP3A4, SULT1E1, and GSTA1 (Fig. S9) and contained components of fatty acid omega oxidation and estrogen metabolism (Table S12). Male portal hepatocytes exhibited a network that included HSP90AA1 and FKBP5 (Fig. 4G), with the proteins in this network predominantly localized to the cytoplasm.

Female sinusoidal endothelial cells showed enrichment of a protein network containing FGA, FGB, and FGG, proteins linked to folate metabolism, the blood clotting cascade, and fibrin complement receptor 3 signaling (Fig. 4H, Table S12). Subcellular localization analysis places this network within the extracellular space. A network containing PIK3R3, IGF1R, HSP90AA1, and PPP2R5C, which are all members of the PI3K/Akt signaling pathway, was enriched in male sinusoidal endothelial cells (Fig. 4I), and these interactions are predicted to occur primarily in the cytosol (Table S12).

Applying machine learning to evaluate male and female cell populations

To determine if liver cells can be classified as female or male by machine learning, we applied a random forest classifier across all cell types (supplementary methods). Two models were trained: a baseline model using all genes (full model) and a second model excluding genes located on the X and Y chromosomes. The full model achieved an accuracy of 81.1% and a recall of 97.9%, while the autosomal model still performed well, with 74.9% accuracy and 97.3% recall (Fig. 4J). We then evaluated classification performance for individual cell types and subtypes (Figs 4K,L, and S12A-I). The full model achieved slightly higher accuracy and recall (Fig. 4K), but the autosomal model showed similar accuracy to all cell types, demonstrating that cell type and subtype classification can be performed using only autosomal gene expression (Table S13, Fig. S12A–I).

When the full model was run, X- and Y-linked genes such as *XIST*, *UTY*, *TTTY14*, and *USP9Y* were among the top features, as expected. *XIST*, known for its critical role in X-chromosome inactivation in females,[11] also exhibited the highest feature importance score. However, even after excluding X and Y chromosome genes, the classifier highlighted key genes contributing to sex differences within the liver, including *CUX2* (Fig. 4M).

We found higher *CUX2* expression in males, contrasting with murine studies reporting female-enriched hepatic *CUX2*.[12]

neighborhood evidence, Blue: co-occurrence evidence, Purple: experimental evidence, Yellow: text mining evidence, Light blue: database evidence, Black: co-expression evidence). (E) Protein network in female portal hepatocytes enriched in pathways related to lipid metabolism. (F) Protein network in female portal hepatocytes enriched in estrogen signaling. (G) Protein network in male portal hepatocytes. (H) Protein network in female sinusoidal endothelial cells. (I) Protein network in male sinusoidal endothelial cells. (J-L) Machine learning-based sex prediction using (J) all cell types combined, (K) portal hepatocytes, and (L) sinusoidal endothelial cells. The blue line indicates the AUC for models trained on all genes (including X and Y chromosomes), while the red line represents models trained exclusively on autosomal genes. (M) The plot shows the top 10 features for predicting sex in the Complete Genome Model (blue bars) and the Autosomal Gene Model (red bars). The y-axis represents feature importance scores, with higher values indicating greater contribution. L-R, ligand-receptor; qHSCs, quiescent hepatic stellate cells; VV, venous vascular.

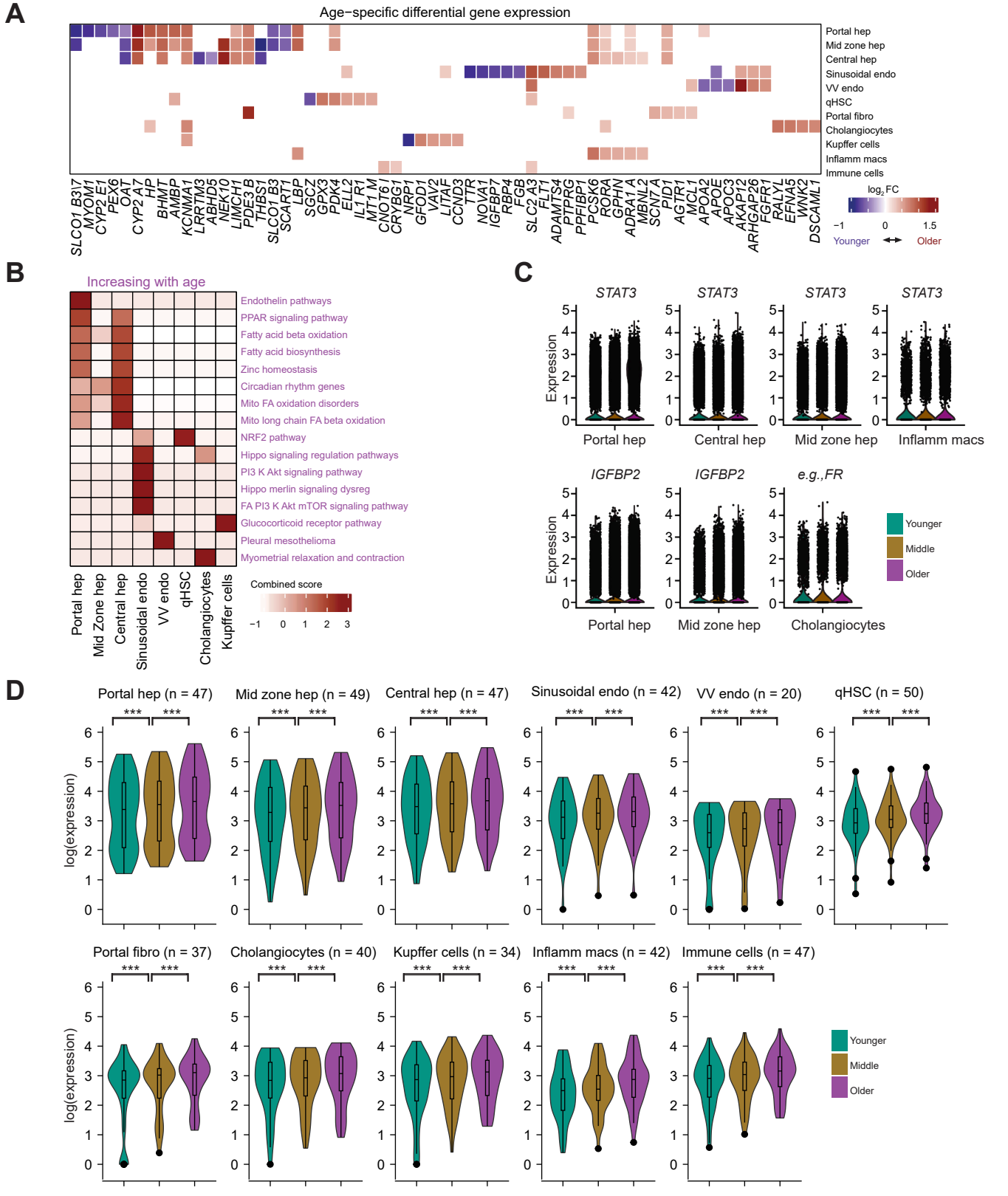

Fig. 5. Age-related gene expression changes and senescence signatures. (A) Heatmap displaying the log_2FC in gene expression between age groups across cell types. Red indicates increased expression with age, and blue decreased expression with age. A maximum of 5 differentially expressed genes, upregulated in each group (increasing or decreasing with age) and expressed in at least 25% of cells are displayed for each cell type and subtype. Genes were called significant in each cell type if detected in ≥10% of cells in either group (min.pct = 0.1), showed $|log_2FC| \geq 0.25$, and had Bonferroni-adjusted *p*-values (p_val_adj) ≤0.1. (B) Heatmap of Gene Ontology-enrichment analysis for upregulated genes across different age groups, focusing on pathways that increase with age. Enrichr combined score is calculated by the logarithmic transformation of the *p* value obtained from Fisher's exact test, multiplied by the z-score. Functional categories were considered

To validate this observation, we examined bulk RNA-seq data.[13] Among 14 tissues with detectable *CUX2* expression (median transcripts per million >1), the liver and several brain regions showed male-biased expression (Fig. S13, Table S14), while a few tissues, including the amygdala and substantia nigra, showed female-biased medians.

To evaluate whether the accuracy of sex prediction was influenced by donor age, we repeated the analysis using only autosomal genes within three age groups (supplementary methods). Nuclei sex was predicted with 86.3% accuracy and 100% recall in younger donors, 82.9% accuracy and 98.4% recall in middle-aged donors, and 87.0% accuracy and 93.4% recall in older donors (Table S15).

Effect of age on differential gene expression and biological pathways

We next investigated how gene expression changes with age across cell types (Fig. 1B and S1). We performed differential expression analysis, using donor and sex as covariates (Table S16). We identified 478 genes that increase in expression from younger to middle-aged to older groups, and 50 genes that decrease with age when analyzed by cell types and subtypes. The top five most enriched genes in older (red) *vs*. younger cells (blue) for each cell type are shown (Fig. 5A).

Pathways enriched with increasing age were also identified (Fig. 5B), with those related to fatty acid metabolism enriched in aging hepatocytes, and hippo signaling and PI3K-Akt signaling enriched in sinusoidal endothelial cells. qHSCs showed significant enrichment for the NRF2 pathway, and the glucocorticoid receptor pathway was enriched in Kupffer cells. Fewer pathways were identified as enriched at a younger age due to the smaller number of genes in this group, but lipid particle composition and cholesterol metabolism pathways were enriched in VV endothelial cells in younger donors (Table S17).

While data on menopause were not available for female donors, we attempted to gain insight into possible effects of menopause by comparing female donors ≤40 years of age with donors >60 years of age (Table S18). These ages were selected because the mean age of menopause is 51.4 years, with <10% of women reaching menopause after age 56 and <2.5% reaching menopause before the age of 45.[14] Younger donors showed enrichment in estrogen metabolism signaling and lipid/PI3K–AKT–mTOR programs, whereas older donors showed enrichment in fatty acid beta-oxidation, cholesterol biosynthesis, and glycolysis (Table S19). A parallel analysis in males revealed similar age-related shifts, with fatty acid β-oxidation, cholesterol production, familial hyperlipidemia type 2, and PPAR signaling enriched in older males. The pathways shared between aging female and male liver cells support aging, rather than menopause, as the primary driver of these changes (Tables S20 and S21).

Senescence signatures with increasing age

Expression of senescence genes increases with age in many organs, but we did not identify a senescence signature in our pathway analysis (Fig. 5B). We next evaluated expression of senescence genes[15] to understand how these genes change with increasing age across cell types and subtypes. *STAT3* was enriched with age in hepatocytes and inflammatory macrophages (Fig. 5C), consistent with the induction of *STAT3* in cellular senescence in liver fibrosis and in senescent macrophages.[16] Genes induced with age also included *IGFBP2* in portal and mid-zone hepatocytes, *EGFR* in portal hepatocytes and cholangiocytes, and *NRG1* in portal hepatocytes (Fig. 5C and S14). While only seven senescence-associated genes were significantly enriched with age within individual cell types or subtypes, different combinations of senescence genes followed the trend of increasing expression from younger to middle to older age groups for each cell type and subtype (Table S22 and supplementary methods). Using the set of genes that increase with age within each cell type and subtype, we then defined cell-type-specific senescence signatures (Fig. 5D, Table S22).

Impact of age on cell-cell communication

Pathways involving IGF, THBS, and CHEMERIN were enriched in younger donor cells (Fig. 6A, green labels), while pathways related to ICAM, SPP1, SEMA6, and NRG were enriched in older donor cells (purple labels). Additional pathways (black labels) were active but did not differ significantly between younger and older cells (Table S23). The IGF pathway shows robust signaling from hepatocytes to sinusoidal and VV endothelial cells, with signaling to qHSCs and portal fibroblasts absent in older cells (Fig. 6B). In contrast, cells from older donors show enrichment in the NRG pathway (Fig. 6C).

To better understand the individual molecules responsible for these cell-cell interactions, we next visualized L-R pairs (Fig. 6D-G, Table S23). L-R pairs containing the ligands IGF1 and VEGFA that signal from portal hepatocytes are enriched in younger donors (Fig. 6D), while L-R pairs containing the ligands NRG1 and PLG that signal from portal hepatocytes were enriched in older donors (Fig. 6E). In younger donors, L-R pairs containing the ligands LAMA3, FLRT2, and collagens signal to portal hepatocytes (Fig. S15A). In older donors, L-R pairs containing BMP-5/6 are expressed by portal fibroblasts and sinusoidal endothelial cells, which signal to portal hepatocytes (Fig. S15B).

significantly enriched at a Benjamini-Hochberg FDR ≤0.1 with ≥3 contributing genes. (C) Violin plots show gene expression in Younger, Middle, and Older donors for senescence-associated genes[15] with significant age-related changes (Table S16). Genes were considered significant within a cell type if detected in ≥10% of cells in either younger or older groups (min.pct = 0.1), $|\log_2 FC| \geq 0.25$, and Bonferroni-adjusted $p\_val\_adj \leq 0.1$ for younger *vs*. older, with middle-aged group expression required to fall between younger and older levels. (D) Cell type-specific senescence signatures. Violin plots of senescence gene expression across indicated groups, with average expression values displayed on a log scale. ***p <0.001 as obtained from pairwise Wilcoxon tests (Materials and methods). FC, fold change; FDR, false discovery rate; qHSCs, quiescent hepatic stellate cells; VV, venous vascular.

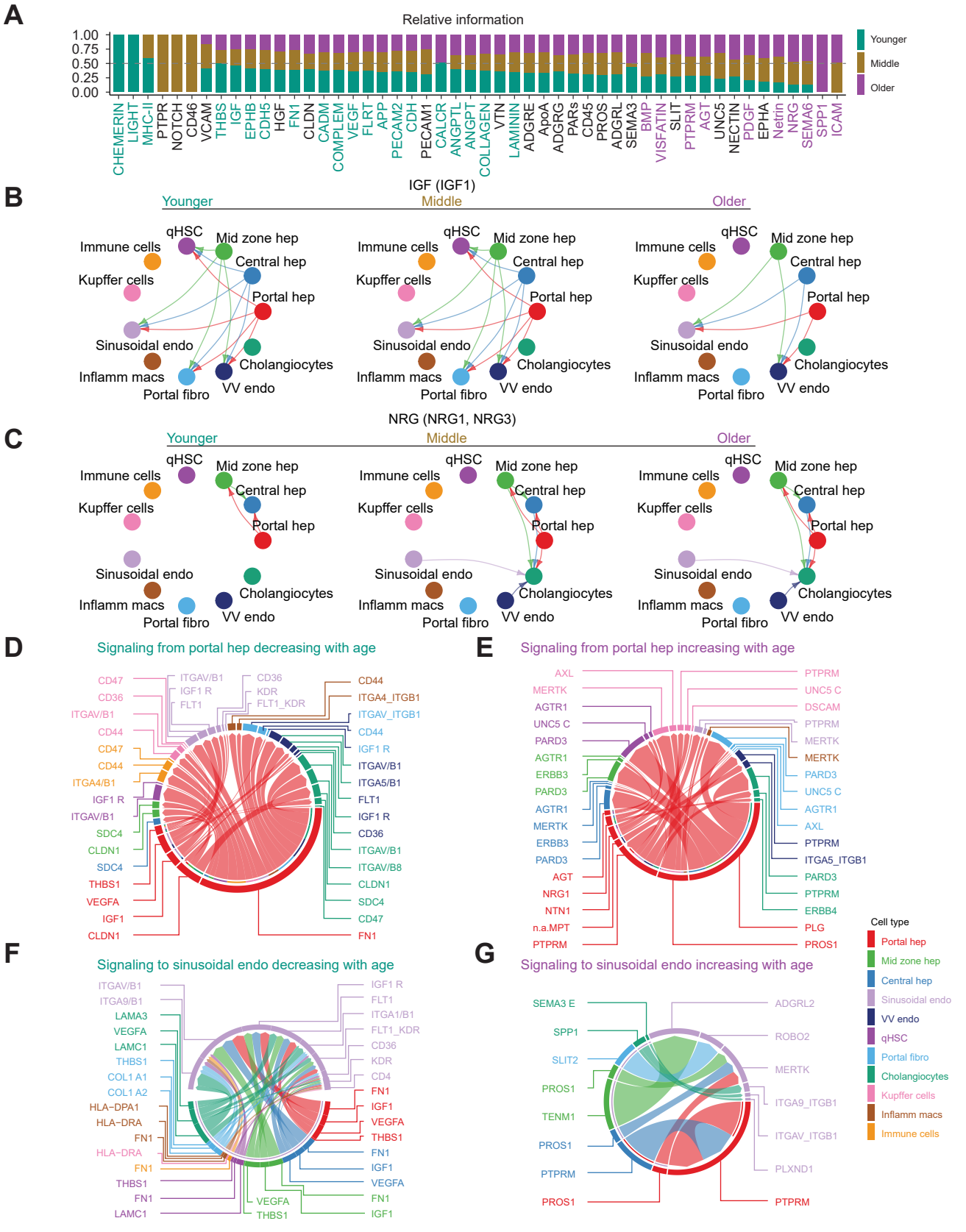

Fig. 6. Age-related changes in signaling pathways and ligand-receptor interactions. (A) Signaling pathways were ranked according to differences in overall information flow within inferred networks across younger, middle-aged, and older populations. Statistical significance was assessed using a paired Wilcoxon test between the yonger and older groups, with $p \leq 0.05$ considered signficant. Pathways labeled in purple are more enriched in older age groups. Pathways labeled in teal are more enriched in younger individuals. Pathways labeled in black show no significant enrichment between younger and older cells. (B) The chord circle plot

Analysis of L-R pairs involving sinusoidal endothelial cells also displayed age-dependent shifts (Fig. 6F,G and S15C,D). In younger donors, L-R pairs containing the ligand THBS1, which signal to sinusoidal endothelial cells, were enriched (Fig. 6F). In older donors, L-R pairs containing the ligands SPP1 and SEMA3C, PROS1, and TENM1 that signal to sinusoidal endothelial cells were enriched (Fig. 6G). L-R pairs containing the ligands EFNB2 and ANGPT2 were enriched in sinusoidal endothelial cells from younger donors (Fig. S15C), while L-R pairs containing the ligands NRG3, ADM, and NAMPT were enriched in sinusoidal endothelial cells from older donors (Fig. S15D).

Discussion

The liver plays a key role in numerous physiological processes. While single-cell studies have highlighted the diversity of liver cell types and disease-related changes,[1–3] the influence of sex and age on healthy liver cell types remains poorly understood. Using snRNA-seq, we analyzed over 195,000 nuclei from 37 adult donors spanning seven decades of life to explore liver cell composition and heterogeneity across sex and age.

Female hepatocytes exhibited broader enrichment of estrogen-related and lipid/lipoprotein pathways, consistent with increased fatty acid oxidation and greater protection from steatosis and metabolic dysfunction-associated steatotic liver disease (MASLD).[17,18] The ferroptosis pathway was also enriched in central hepatocytes in females, while TGF-β signaling was more enriched in midzone and portal hepatocytes, suggesting pathways that could influence sex-linked differences in injury responses and fibrosis/repair dynamics.[19,20] In males, enrichment of chemokine signaling, glucocorticoid receptor programs, and Hippo signaling point to pathways that may contribute to the higher burden of MASLD/MASH and metabolic comorbidities.[21]

While common pathways were observed in aging for both males and females, indicating general aging, the analysis also revealed pathway shifts consistent with hepatic masculinization in older females. Younger female cells were enriched for estrogen-linked programs and sulfatase and aromatase pathways, alongside omega fatty acid synthesis, and modulation of PI3K Akt mTOR signaling, consistent with pre-menopausal physiology.[22,23] In contrast, older females gained male-biased programs, including androgen receptor network, SREBP signaling, cholesterol biosynthesis pathway/hepatocytes, and urea cycle and associated pathways, and these pathways were all enriched in younger compared to older males (Tables S18–S21). The convergence of pathways enriched in older females with those associated with male-anchored axes supports a shift toward a male-like hepatic state as estrogen signaling declines. This interpretation aligns with evidence that declining hepatic estrogen receptor-α after menopause promotes transcriptomic masculinization[24] and with animal data showing higher plasma cholesterol in low-estrogen females.[25]

BMP emerged as a male-enriched signaling pathway (Fig. 3G), driven by BMP6 expression in sinusoidal endothelial cells signaling to qHSCs, with weaker signals to hepatocytes, cholangiocytes, and portal fibroblasts.[26] BMP6 is induced with MASLD and has activity against inflammation and fibrosis,[27] in addition to its role in regulating hepcidin expression in hepatocytes.[28] Beyond iron homeostasis, BMP6 also suppresses hepatic fibrosis in MASLD,[27] highlighting its broader role in liver metabolism and pathology. Together, these findings highlight pathways by which enrichment of BMP6 signaling in males may influence susceptibility to MASLD and related liver diseases.

Machine learning revealed distinct autosomal gene expression differences (Table S13). *FKBP5* shows sex-dependent expression influenced by hormonal environments.[29] A2M is estrogen-responsive and consistently expressed at higher levels in females,[30] while PZP is a pregnancy-associated protein regulated by estrogen and progesterone.[31] PPARGC1A also shows differences in expression by sex, shaped by metabolic and hormonal inputs.[32] Our analysis of GTEx data further supports the conclusion that CUX2 is enriched in the male liver (Fig. S13, Table S14). These findings open avenues for further research into the intricate biological pathways that govern sex differences at the cellular level.

Age-related shifts revealed that younger livers show enriched IGF and VEGFA signaling. IGF and its receptor IGF1R prevent apoptosis, promote cell proliferation, and induce VEGF expression.[33] VEGFA regulates angiogenesis, inflammatory responses, and energy metabolism, including hepatic lipid and glycogen metabolism.[34] In contrast, older livers exhibit increased NRG1 and PLG signaling, suggesting adaptations in repair and metabolism. NRGs regulate glucose and lipid homeostasis[35] and protect against MASLD by modulating ERBB3 phosphorylation and PI3K-AKT signaling.[36] These findings highlight age-related shifts from growth and vascular signals in younger livers to repair-focused signaling in older livers.

While this study provides insights into sex- and age-related differences within the liver, limitations exist. The cohort of 37 adult donors, mostly Caucasian (35), may limit generalizability to broader populations. Samples from a single center reflect local geography, and although histologically assessed as healthy, tissues were derived from excess surgical samples, potentially not representing completely healthy livers. Covariate-adjusted analyses were performed to control for age and sex, but the assignment of age by decade to each sample prevented exact age matching between donors. While we attempted to approximate menopausal status by comparing women ≤40 years and >60 years, this approach cannot fully capture the heterogeneity of reproductive aging and associated hormonal changes. Despite these constraints, the study

illustrates IGF signaling pathways with enriched ligand (IGF1) across cell types in younger, middle-aged, and older populations. Colors indicate cell-type expressing the ligand. Strength of communication is indicated by the thickness of the line, and arrows indicate direction. (C) NRG signaling with enriched ligands (NRG1 and NRG3) across age groups. (D-G) Chord diagrams represent aging-specific L-R interactions. Outer rings denote different cell types, while the links illustrate interactions, with ligands expressed by the source cell type and receptors expressed by the target cell type. L-R signaling originating from portal hepatocytes enriched with decreased (D) and increased age (E) L-R signaling to sinusoidal endothelial cells enriched with decreased (F) and increased age (G). L-R, ligand-receptor; qHSCs, quiescent hepatic stellate cells; VV, venous vascular.

highlights the broad influence of sex and age on liver cell types and subtypes.

In conclusion, our snRNA-seq analysis reveals sex- and age-related changes in gene expression, signaling, and cell-cell communication in the healthy human liver at the cell-type and subtype level. These findings offer a reference for studying the impact of sex and age on liver disease progression. Future studies incorporating comprehensive clinical covariates such as BMI, metabolic status, and circulating hormone profiles will be required to understand the influence of these factors on cellular functions within the context of sex and age.

Affiliations

[1]*Division of Gastroenterology, University of Massachusetts Chan Medical School, Worcester, MA, USA;* [2]*Broad Institute of MIT and Harvard, Cambridge, MA, USA;* [3]*Division of Gastroenterology, Massachusetts General Hospital, Boston, MA, USA;* [4]*Klarman Cell Observatory, Broad Institute of MIT and Harvard, Cambridge, MA, USA;* [5]*Division of Gastrointestinal and Oncologic Surgery, Harvard Medical School and Massachusetts General Hospital, Boston, MA, USA;* [6]*Division of Pathology, Massachusetts General Hospital, Boston, MA, USA*

Abbreviations

HSCs, hepatic stellate cells; L-R, ligand-receptor; qHSCs, quiescent HSCs; scRNA-seq, single-cell RNA sequencing; snRNA-seq, single-nucleus RNA sequencing; UMAP, uniform manifold approximation and projection; VV, venous vascular.

Financial support

Chan Zuckerberg Initiative (A.C.M.)

Conflicts of interest

A.C.M. has received research funding from GlaxoSmithKline for unrelated projects. R.R. is a co-founder of deepnostiX, based in Germany and Pakistan, and founder of VitalEdge in the USA. Additionally, R. R. serves as a consultant for Ibis Therapeutics. No other authors have conflicts to declare.
Please refer to the accompanying ICMJE disclosure forms for further details.

Authors' contributions

R.R., J.D., and A.C.M. conceived the study and designed the experiments. Samples were collected following patient consent and prepared for analysis by E.T.E., H.K., and L.F., with additional assistance from A.S., K.T., M.Q., C.F., D.B., and C.F.C. snRNA-seq was performed by L.A.-Z., S.M., and C.L. with support from J.D. Computational analyses were performed by R.R. The manuscript was written by R.R. and A.C.M. with input from all authors.

Declaration of AI-assisted technologies in the writing process

The authors used ChatGPT to generate alternative versions of individual sentences, from which elements were chosen to improve clarity. The authors reviewed and edited the content as needed and take full responsibility for the content of the publication.

Data availability

Sequencing data used for this study are included in the Gene Expression Omnibus (GEO) under accession code: GSE210077 and on UCSC Cell Browser[37] under https://liver-sex-age-map.cells.ucsc.edu.

Acknowledgements

The authors thank Ramnik Xavier and Åsa Segerstolpe for helpful discussions, Jasneet Aneja, Helena Lau, Georg Lauer, Stefan Gentile, Carlos Fernandez-del Castillo, and Genevieve Boland for assistance with collection of liver tissue and Jonathan Eddy, Oiza Dimowo, James Cheney, and Mantero Valentino Moreno-Cheek for assistance with tissue preservation. We thank Adam Slamin, Salome Maldonado, Dan Dubinsky, and the Broad Genomics Platform for help generating the snRNA-seq data. This publication is part of the Human Cell Atlas - www.humancellatlas.org/publications.

Supplementary data

Supplementary data to this article can be found online at https://doi.org/10.1016/j.jhepr.2026.101773.

References

Author names in bold designate shared co-first authorship

[1] **MacParland SA**, **Liu JC**, **Ma X-Z**, et al. Single cell RNA sequencing of human liver reveals distinct intrahepatic macrophage populations. Nat Commun 2018;9:1–21.
[2] Ramachandran P, Dobie R, Wilson-Kanamori JR, et al. Resolving the fibrotic niche of human liver cirrhosis at single-cell level. Nature 2019;575:512–518.
[3] Aizarani N, Saviano A, Sagar Mailly L, et al. A human liver cell atlas reveals heterogeneity and epithelial progenitors. Nature 2019;572:199–204.
[4] **Slyper M**, **Porter CBM**, **Ashenberg O**, et al. A single-cell and single-nucleus RNA-Seq toolbox for fresh and frozen human tumors. Nat Med 2020;26:792–802.
[5] Ianevski A, Giri AK, Aittokallio T. Fully-automated and ultra-fast cell-type identification using specific marker combinations from single-cell transcriptomic data. Nat Commun 2022;13:1246.
[6] Xu C, Prete M, Webb S, et al. Automatic cell-type harmonization and integration across Human Cell Atlas datasets. Cell 2023;186:5876–5891.e20.
[7] **Halpern KB**, **Shenhav R**, Matcovitch-Natan O, et al. Single-cell spatial reconstruction reveals global division of labour in the mammalian liver. Nature 2017;542:352–356.
[8] **Gómez-Salinero JM**, **Izzo F**, Lin Y, et al. Specification of fetal liver endothelial progenitors to functional zonated adult sinusoids requires c-Maf induction. Cell Stem Cell 2022;29:593–609.e7.
[9] **Yang W**, **He H**, Wang T, et al. Single-cell transcriptomic analysis reveals a hepatic stellate cell-activation roadmap and myofibroblast origin during liver fibrosis in mice. Hepatology 2021;74:2774–2790.
[10] Tamkun JW, Hynes RO. Plasma fibronectin is synthesized and secreted by hepatocytes. J Biol Chem 1983;258:4641–4647.
[11] Pacini G, Dunkel I, Mages N, et al. Integrated analysis of Xist upregulation and X-chromosome inactivation with single-cell and single-allele resolution. Nat Commun 2021;12:3638.
[12] Laz EV, Holloway MG, Chen C-S, et al. Characterization of three growth hormone-responsive transcription factors preferentially expressed in adult female liver. Endocrinology 2007;148:3327–3337.
[13] GTEx Consortium. The genotype-tissue expression (GTEx) project. Nat Genet 2013;45:580–585.
[14] Zhu D, Chung H-F, Pandeya N, et al. Body mass index and age at natural menopause: an international pooled analysis of 11 prospective studies. Eur J Epidemiol 2018;33:699–710.
[15] Saul D, Kosinsky RL, Atkinson EJ, et al. A new gene set identifies senescent cells and predicts senescence-associated pathways across tissues. Nat Commun 2022;13:4827.
[16] Pang X, Gao S, Liu T, et al. Identification of STAT3 as a biomarker for cellular senescence in liver fibrosis: a bioinformatics and experimental validation study. Genomics 2024;116:110800.
[17] Ballestri S, Nascimbeni F, Baldelli E, et al. NAFLD as a sexual dimorphic disease: role of gender and reproductive status in the development and progression of nonalcoholic fatty liver disease and inherent cardiovascular risk. Adv Ther 2017;34:1291–1326.
[18] Hart-Unger S, Arao Y, Hamilton KJ, et al. Hormone signaling and fatty liver in females: analysis of estrogen receptor α mutant mice. Int J Obes (Lond) 2017;41:945–954.
[19] **Yin J**, **Xu X**, Guo Y, et al. Repair and regeneration: ferroptosis in the process of remodeling and fibrosis in impaired organs. Cell Death Discov 2024;10:424.
[20] Qi Z, Atsuchi N, Ooshima A, et al. Blockade of type beta transforming growth factor signaling prevents liver fibrosis and dysfunction in the rat. Proc Natl Acad Sci U S A 1999;96:2345–2349.
[21] Pan X, Chiwanda Kaminga A, Liu A, et al. Chemokines in non-alcoholic fatty liver disease: a systematic review and network meta-analysis. Front Immunol 2020;11:1802.
[22] **Qing T**, **Karn T**, Rozenblit M, et al. Molecular differences between younger versus older ER-positive and HER2-negative breast cancers. NPJ Breast Cancer 2022;8:119.

[23] Ko S-H, Kim H-S. Menopause-associated lipid metabolic disorders and foods beneficial for postmenopausal women. Nutrients 2020;12:202.
[24] Meda C, Benedusi V, Cherubini A, et al. Hepatic estrogen receptor alpha drives masculinization in post-menopausal women with metabolic dysfunction-associated steatotic liver disease. JHEP Rep 2024;6:101143.
[25] Trapani L, Segatto M, Pallottini V. Regulation and deregulation of cholesterol homeostasis: the liver as a metabolic "power station.". World J Hepatol 2012;4:184–190.
[26] Wang S, Chen C, Yu L, et al. Bone morphogenetic protein 6-mediated crosstalk between endothelial cells and hepatocytes recapitulates the iron-sensing pathway in vitro. J Biol Chem 2021;297:101378.
[27] Arndt S, Wacker E, Dorn C, et al. Enhanced expression of BMP6 inhibits hepatic fibrosis in non-alcoholic fatty liver disease. Gut 2015;64:973–981.
[28] **Andriopoulos B Jr**, **Corradini E**, **Xia Y**, et al. BMP6 is a key endogenous regulator of hepcidin expression and iron metabolism. Nat Genet 2009;41:482–487.
[29] Lee RS, Mahon PB, Zandi PP, et al. DNA methylation and sex-specific expression of FKBP5 as correlates of one-month bedtime cortisol levels in healthy individuals. Psychoneuroendocrinology 2018;97:164–173.
[30] Zheng W, Xu H, Lam SH, et al. Transcriptomic analyses of sexual dimorphism of the zebrafish liver and the effect of sex hormones. PLoS One 2013;8:e53562.
[31] Folkersen J, Teisner B, Grunnet N, et al. Circulating levels of pregnancy zone protein: normal range and the influence of age and gender. Clin Chim Acta 1981;110:139–145.
[32] Ruigrok SR, Stöberl N, Yam K-Y, et al. Modulation of the hypothalamic nutrient sensing pathways by sex and early-life stress. Front Neurosci 2021;15:695367.
[33] Reinmuth N, Fan F, Liu W, et al. Impact of insulin-like growth factor receptor-I function on angiogenesis, growth, and metastasis of colon cancer. Lab Invest 2002;82:1377–1389.
[34] Wang Y, Ni J, Wang A, et al. Vascular endothelial growth factor A (VEGFA) regulates hepatic lipid and glycogen metabolism in Schizothorax prenanti. Int J Mol Sci 2023;24:15171.
[35] Zhang P, Kuang H, He Y, et al. NRG1-Fc improves metabolic health via dual hepatic and central action. JCI Insight 2018;3. https://doi.org/10.1172/jci.insight.98522.
[36] Meng D, Pan H, Chen Y, et al. Roles and mechanisms of NRG1 in modulating the pathogenesis of NAFLD through ErbB3 signaling in hepatocytes (NRG1 modulates NAFLD through ErbB3 signaling). Obes Res Clin Pract 2021;15:145–151.
[37] Speir ML, Bhaduri A, Markov NS, et al. UCSC Cell Browser: visualize your single-cell data. Bioinformatics 2021;37:4578–4580.

Keywords: Sex differences; Sexual dimorphism; Aging; Age-associated changes; Human liver: cell–cell communication; Protein–protein interaction networks; Pathway enrichment analysis; Insulin growth factor (IGF); Neuregulin (NRG); Cellular senescence; Healthy reference atlas.

Received 28 February 2025; received in revised form 7 January 2026; accepted 29 January 2026; Available online 11 February 2026